Front. Optoelectron. 2018, 11(3): 245–255
https://doi.org/10.1007/s12200-018-0820-2

RESEARCH ARTICLE

Longitudinal twinning α-In_2Se_3 nanowires for UV-visible-NIR photodetectors with high sensitivity

Zidong ZHANG[1,2], Juehan YANG[1], Fuhong MEI[2], Guozhen SHEN (✉)[1,3]

1 State Key Laboratory for Superlattices and Microstructures, Institute of Semiconductors, Chinese Academy of Sciences, Beijing 100083, China
2 Key Laboratory of Interface Science and Engineering in Advanced Materials of Ministry of Education, Research Center of Advanced Materials Science and Technology, Taiyuan University of Technology, Taiyuan 030024, China
3 College of Materials Science and Opto-electronic Technology, University of Chinese Academy of Sciences, Beijing 100029, China

Abstract Longitudinal twinning α-In_2Se_3 nanowires with the $(10\bar{1}\,8)$ twin plane were synthesized to fabricate high performance single nanowire based photodetectors. As-synthesized α-In_2Se_3 nanowire exhibited typical n-type semiconducting behavior with an electron mobility of 23.1 $cm^2 \cdot V^{-1} \cdot S^{-1}$ and a broadband spectral response from 300 to 1100 nm, covering the ultraviolet-visible-near-infrared (UV-visible-NIR) region. Besides, the fabricated device showed a high responsivity of 8.57×10^5 $A \cdot W^{-1}$, high external quantum efficiency up to 8.8×10^7% and a high detectivity of 1.58×10^{12} Jones under 600 nm light illumination at a basis of 3 V, which are much higher than previously reported In_2Se_3 nanostructures due to the interface defect effect of the twin plane. The results indicated that the longitudinal twinning α-In_2Se_3 nanowires have immense potential for further applications in highly performance broadband photodetectors and other optoelectronic devices.

Keywords photodetectors, nanowires, twinning, ultraviolet-visible-near-infrared (UV-visible-NIR)

1 Introduction

Photodetectors, widely applied in optical communication, optical switches and high-resolution imaging techniques, have aroused great attention for decades [1–3]. With high specific surface, special geometry and confined quantum effect, semiconductor nanowires serve as essential candidates for realizing high performance photodetectors and many kinds of semiconducting nanowires have been utilized to fabricate photodetectors responsing to light with different wavelengths [4–12]. Among the semiconducting nanowires, binary chalcogenide $A_2^{III}B_3^{VI}$ (A = In and B = S, Se, Te) nanowires are thought to be good candidates for photodetectors because the mismatch between III and VI atoms can adjust nanowires' morphology and further provide the opportunity to engineer materials for better device performance [13–16]. Particularly, indium selenide (In_2Se_3) nanowires have been applied to fabricate photodetectors because of the highly anisotropic structural, excellent electrical, optical and mechanical characteristics [17–26]. In_2Se_3 nanowires usually show response to broad-spectrum light from ultraviolet (UV), visible to near-infrared (NIR), which is beneficial for extending the range of photodetectors application.

For the nanowires used for photodetectors, researchers found that defects, such as twinning, stacking faults, vacancies, etc., have great effects on their performance. Twinning as one of the most important kinds of defects, has been widely found in many groups of semiconducting nanowires, such as III-V nanowires [27–30], II-VI nanowires [31–33], and many other semiconductor materials including Zn_2SnO_4, Zn_3P_2, Zn_2GeO_4 [34–36]. It is predicted that twinning can induce electronic miniband structure, which may be used to adjust the electronic and photoelectric properties of nanowires [37–40]. However, for III-VI group semiconducting nanowires, till now, the twinning, including longitudinal twinning, has seldom been reported due to the difficulties in materials synthesis, not to mention the influence of twinning on the optoelectronic performance of photodetectors.

Received April 4, 2018; accepted May 3, 2018

E-mail: gzshen@semi.ac.cn

Invited Paper

In this work, by controlling experimental parameters, longitudinal twinning α-In_2Se_3 nanowires were successfully synthesized by a conventional chemical vapor deposition (CVD) method. Afterwards, the single twinned In_2Se_3 nanowire based photodetectors were fabricated. Studies found that the as-synthesized α-In_2Se_3 nanowires exhibited typical n-type semiconducting behavior with an electron mobility of 23.1 $cm^2 \cdot V^{-1} \cdot S^{-1}$ and a broadband spectral response from 300 to 1100 nm, covering the UV-visible-NIR region, with high responsivity, stability, and reproducibility, which are attributed to the interface defect of the twin plane. Our results indicated that the n-type longitudinal twinning α-In_2Se_3 nanowires had immense potential for further applications in the broadband spectral detectors from UV-visible-NIR light.

2 Experimental section

The longitudinal twinning α-In_2Se_3 nanowires were synthesized via a facile CVD method in a horizontal quartz tube. In a typical process, 0.030 g of pure In_2Se_3 powder (Alfa Aesar, 99.99%) was put in an alumina boat at the center of a tube furnace as the source material. A Si wafer covered with 5 nm thick Au film, acting as the catalysts for the growth of nanowires, was placed on another alumina boat located downstream 15 – 17 cm away from the center. After the tube was purged with ultra-pure argon for 30 min to eliminate oxygen, the tube was heated to 940°C – 950°C in 35 min and kept at the temperature for 1 h. The flow rate of the carrier gas (Ar) was kept at 30 sccm (standard cubic centimeters per minute). After cooled to room temperature, a layer of shiny silver-gray product was found deposited on Si substrate. The as-prepared nanowires were characterized by X-ray diffraction (XRD, Rigaku D/Max-2550, λ = 1.5418 Å), scanning electron microscopy (SEM, Zeiss Supra55(VP)), and transmission electron microscopy (TEM, Tecnai G2 F20, FEI) with an energy-dispersive X-ray (EDX) analyzer.

To fabricate single In_2Se_3 nanowire-based photodetectors, the as-synthesized nanowires were transferred to a SiO_2/Si substrate (300 nm thick SiO_2 on p-type heavily-doped Si) by the contact printing method. Subsequently, using the standard photolithography, thermal evaporation and lift-off process, the Ti/Au (10/60 nm) electrodes were patterned on top of the nanowires, where the channel length (L) is 10 μm. The electronic and optoelectronic properties of the devices were measured by the four probe station connected with the Keithley 4200-SCS semiconductor characterization. A power adjustable homogeneous light source system was used as the illumination source for the measurements. The incident power of the light was measured by an Ophir NOVA power meter. All measurements were completed at room temperature.

3 Results and discussion

Figure 1(a) displays the scanning electron microscope (SEM) image of the synthesized product, which shows the formation of nanowires with an average length of tens of micrometers. The inset image of Fig. 1(a) shows that the top of the nanowire has Au particle, indicating a typical vapor-liquid-solid (VLS) growth mechanism. A high-magnification SEM image of a single nanowire is shown in Fig. 1(b), indicating the diameter of the nanowire is ca. 120 nm. Figure 1(c) shows the X-ray diffraction (XRD) pattern of the as-prepared nanowires. All the diffraction peaks can be indexed to the hexagonal α-In_2Se_3 phase (JSPDS: 34-1279), indicating the formation of pure α-In_2Se_3 products. The compositions of the nanowire are investigated by energy dispersive spectrometer (EDS) and EDS mapping, as presented in Figs. 1(d) and 1(e). From the results, the synthesized nanowires are confirmed to be composed of pure In and Se elements. X-ray photoelectron spectroscopy (XPS) was also performed to confirm the composition of the nanowires, as shown in Fig. S1 (Supporting Information). From the full-scale XPS spectrum (Fig. S1(a)), the spectral characteristic peaks clearly indicate the formation of indium selenide. The In 3d and Se 3d doublets well demonstrate the chemical valence of In and Se in In_2Se_3 nanowire. The signal of C and O come from the atmosphere. The stoichiometric ratios of In and Se estimated by the XPS analysis in Figs. S1(b) and S1(c) are 2:3, confirming the formation of pure In_2Se_3 nanowires.

Figures S2(a) and 1(f) show the TEM images of several typical In_2Se_3 nanowires. Distinct twin planes are clearly observed along the nanowires, indicating the formation of twinned nanowires in the experiments. The high-resolution TEM (HRTEM) images taken from the two parts marked in Fig. 1(f) are shown in Figs. 1(g) and 1(h). The results revealed that the two sides of the twin plane in the nanowire have perfectly crystalline with the similar lattice fringes of 0.97 nm, corresponding to the d-spacing of the (0002) plane of hexagonal In_2Se_3 structure. The selected area electron diffraction (SAED) patterns in Fig. 1(i) of the twinned nanowire clearly show the structure relationship of the twinning, which can be indexed as the $\langle 1\bar{2}10 \rangle$ or $\langle 01\bar{1}0 \rangle$ zone axis. The twin plane of the In_2Se_3 nanowire is thus $(10\bar{1}8)$. The measured angle between the $(10\bar{1}0)$ plane or the $(10\bar{1}0)_t$ plane (subscript t stands for the corresponding twinning) is about 55°. The formation of twinned In_2Se_3 nanowires in this work may be caused by the higher reaction temperature and lower carrier gas flow. Compared with previous reports [15,22], which may lead to the likelihood of twin formation, similar to previous report on twinned III-V nanowires [41]. Due to the relatively low twinning energies, higher growth temperatures can unex-

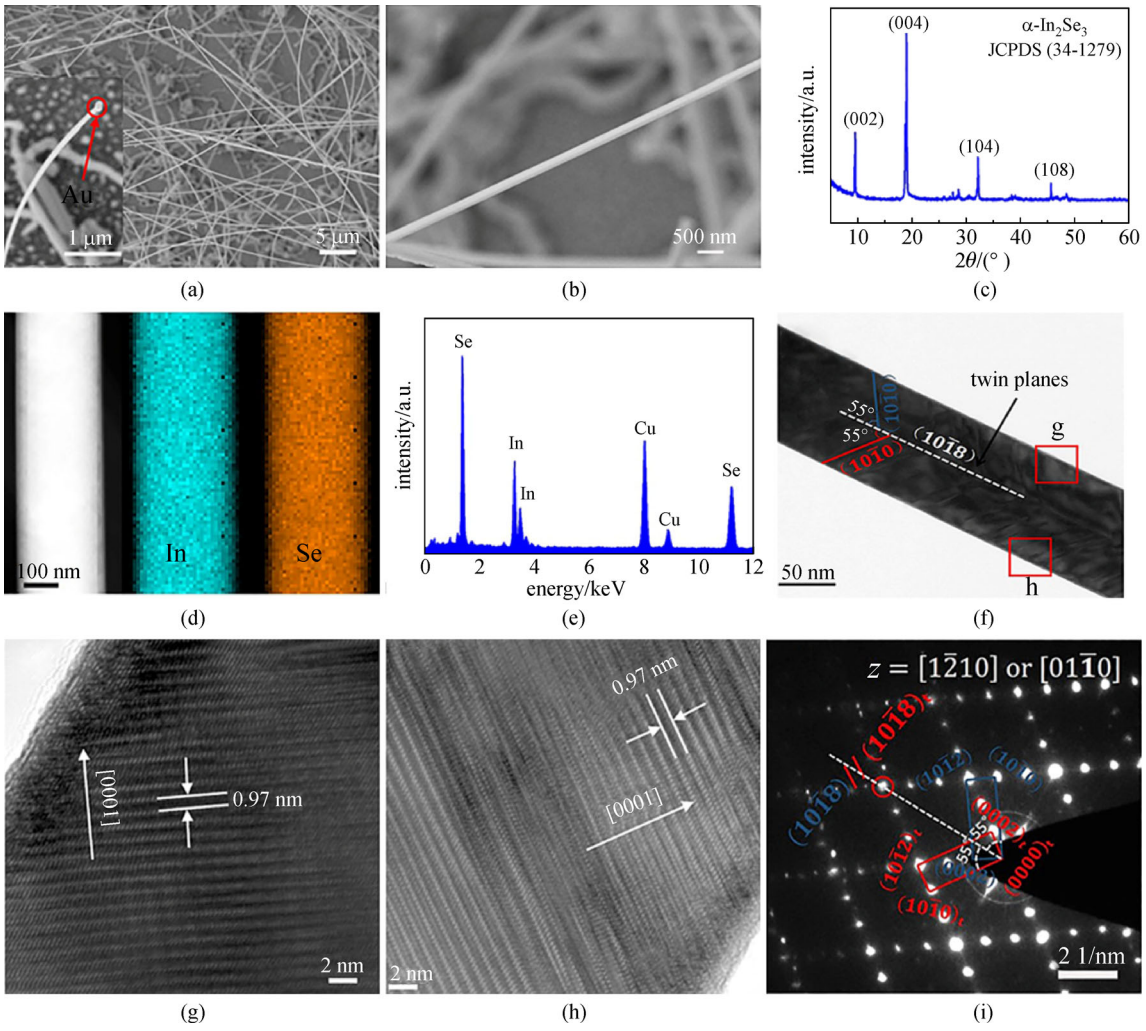

Fig. 1 (a) and (b) SEM images; (c) XRD pattern; (d) elemental mapping; (e) EDS spectrum; (f) TEM image; (g) and (h) HRTEM images; and (i) SAED pattern of the as-synthesized In_2Se_3 nanowires (NWs)

pectedly lead to an increased number of interfacial defects. And the lower Ar gas flow brings less reagents, resulting in twin plane along the axial transmission.

To determine the electronic transport properties of the longitudinal twinning In_2Se_3 nanowire, single nanowire field-effect transistors (FETs) are then fabricated on p-type degenerately doped Si substrate covered with a 300 nm thick SiO_2 layer. As shown in Fig. 2(a), the source-drain current (I_{ds}) increases with the increased back gate voltage (V_{gs}) from –40 to 40 V, revealing a typical n-type semiconducting behavior [15]. Figure 2(b) plots the corresponding transfer curve measured from –40 to 40 V at a source-drain voltage (V_{ds}) of 5 V. The electron mobility (μ_e) of the device can be estimated via the following equation [42]:

$$\mu_e = g_m L^2/(V_{ds}C_i), \quad (1)$$

where C_i is the capacitance of the back gate, L = 10 μm is the length of the device channels and g_m is the transconductance. C_i can be estimated from

$$C_i = 2\pi\varepsilon_0\varepsilon_s L/\mathrm{In}(2h/r), \quad (2)$$

where $\varepsilon_0 = 8.85 \times 10^{-12}$ F·m^{-1} is the vacuum dielectric constant, $\varepsilon_s = 3.9$ is the relative dielectric constant of SiO_2, h = 300 nm is the thickness of the SiO_2 layer, and r = 120 nm is the radius of the nanowire. The calculated C_i of our device is about 1.35×10^{-15} F. Meanwhile, the transconductance is the slope of the curve on the transfer characteristic curve and can be expressed as $g_m = dI_{ds}/dV_{ds}$. From the transfer curve of the device, the g_m is calculated as 0.156 μA·V^{-1}. Hence, the μ_e of the synthesized longitudinal twinning In_2Se_3 nanowire is about 23.1 cm^2·V^{-1}·S^{-1}.

According to previous reports, twinning, as one of the most important kinds of defects, usually leads to different optoelectronic performance compared with conventional

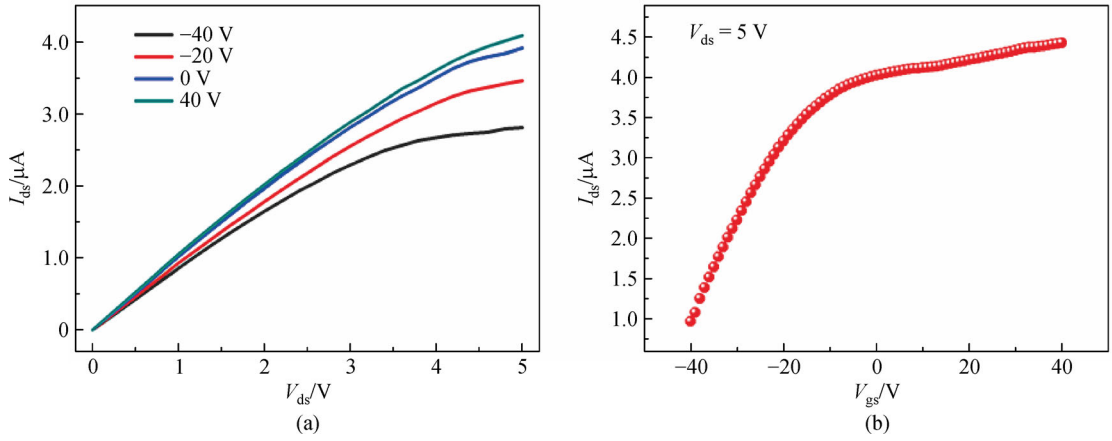

Fig. 2 (a) Output curves of single In_2Se_3-basedtwinning nanowire FET; (b) transfer curve of single In_2Se_3-based twinning nanowire FET at a bias of 5 V

single-crystalline nanowires. In general, twinned nanowires can be divided into transverse twinned and longitudinal twinned nanowires determined by whether the twinning planes are vertical or parallel to the axis of the nanowires, respectively. The electronic performance of transverse twinned nanowires is deteriorated because of the blocking of the twinning interfaces while it is strengthened for the longitudinal twinned nanowires [35–40]. To study the optoelectronic properties of the synthesized longitudinal twinning In_2Se_3 nanowires, single nanowire photodetectors are then fabricated and Fig. 3(a) is the structure of the corresponding device. SEM image of the device is shown in the inset of Fig. 3(b), where Ti/Au top electrodes are patterned via thermal evaporation. The photoresponse characteristics of the device under homochromatic light excitation are shown in Figs. 3(b)–3(f). Figure 3(b) depicts the current-voltage (*I-V*) curves of the device under several typical conditions, namely, dark, 300 nm UV light, 600 nm visible light and 800 nm NIR light illumination, respectively. The device showed response to all the light illuminations as revealed by the curves. Figure 3(c) exhibits the *I-V* curves of the device under 600 nm visible light illuminations with different power intensities. For the input light intensities (3.06–8.84 $\mu W \cdot cm^{-2}$), the photocurrent was found to increases gradually with increased light intensities. The correlation curve of photocurrent I_{ph} ($I_{ph} = I_{illumination} - I_{dark}$) versus incident light power (P) at a bias voltage of 3 V is plotted, as shown in Fig. 3(d), where I_{ph} is proportional to P^r (r is a proportionality value) with r = 0.99 by fitting the experimental values. The r value, reflecting the photocurrent efficiency, is very close to 1, suggesting the excellent photocurrent capability of the longitudinal twinning In_2Se_3 nanowires under visible spectral range. The right vertical axis of Fig. 3(d) is the responsivity (R_λ), which is a crucial parameter to evaluate the sensitivity of the device. R_λ can be defined as the photocurrent (I_{ph}) generated per unit power of the incident light on the effective area (S) of the photodetector, calculated by the following equation

$$R_\lambda = I_{ph}/(PS), \tag{3}$$

where P is the incident light power intensity [7]. The responsivity at 3 V is thus measured to be up to 8.57×10^5 $A \cdot W^{-1}$ at the incident light power intensity of 3.06 $\mu W \cdot cm^{-2}$, and the R_λ deceases as the power intensity of light increases. Because of the increase of photogenerated holes, the density of the trap states on nanowire surface will further decrease with the increase of the light energy. After the trap states are completely filled, the new photogenerated holes and electrons will recombine immediately (within several tens of picoseconds), thus they will not take part in the charge transfer process [43,44]. Therefore, R_λ show a downward trend as the light intensity further increases.

External quantum efficiency (EQE) and detectivity (D^*) are another two crucial parameters used to evaluate the performance of photodetectors. EQE can be calculated using the formulas

$$\mathrm{EQE} = hcR_\lambda(e\lambda), \tag{4}$$

where c is velocity of light, h is the Plank's constant, e is the absolute value of electron charge (1.6×10^{-19} C), and λ is exciting light wavelength [13]. Detectivity (D^*), reflecting the sensitivity of a photodetector to incident light, can be expressed as [13]

$$D^* = R_\lambda S^{1/2}(2eI_{dark})^{1/2}, \tag{5}$$

where I_{dark} is the source-drain current without light illuminations.

Hence, the EQE and D^* of our device are calculated as up to 8.8×10^7% and 1.58×10^{12} Jones, respectively. The curves of EQE and D^* versus P at a bias voltage of 3 V is

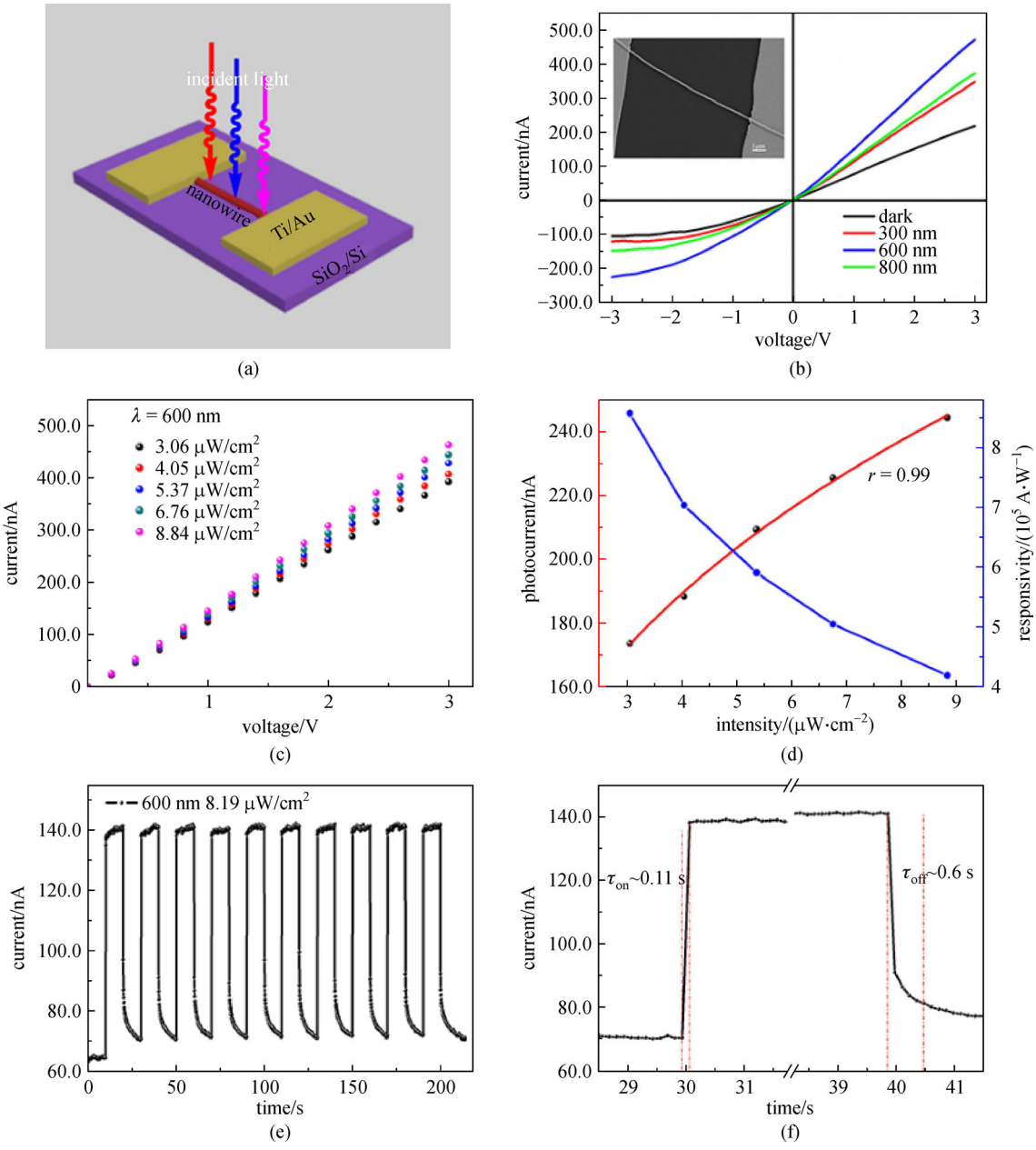

Fig. 3 (a) Schematic illustration of the single nanowire photodetector. (b) *I-V* curves of the device in the dark and under illumination with light of different wavelengths. (c) *I-V* curves of the device under 600 nm light illumination with different power intensities. (d) Photocurrent and responsivity as a function of light power intensity. The fitting result is $I_{ph} \sim P^{0.99}$. (e) Time-resolved photoresponse of the device recorded for a power density of 8.19 μW·cm^{-2}. (f) Response and recovery times of the device

plotted in Fig. S3. The EQE and D^* reveal a downward trend with further increased light intensity.

The stability of the photodetector is another important figure-of-Merit, which is checked by a 600 nm light switched on and off with the power intensity of 8.19 μW·cm^{-2} at a fixed voltage of 1 V. As shown in Fig. 3(e), the "ON" and "OFF" states repeated for ten times still keep the same current level, suggesting the single nanowire photodetector has excellent stability and reversibility. Figure 3(f) presents the single-cycle response of the device under light ON and OFF state, respectively. The device shows fast response to light irradiation and the measured rising time (τ_{on}) and decay time (τ_{off}) are 0.11 s and 0.6 s, respectively.

Broadband photodetectors with the ability to detect lights with wide wavelengths ranging from UV, visible to NIR is particularly important for varied scientific and industrial applications. As an n-type III-VI semiconductor

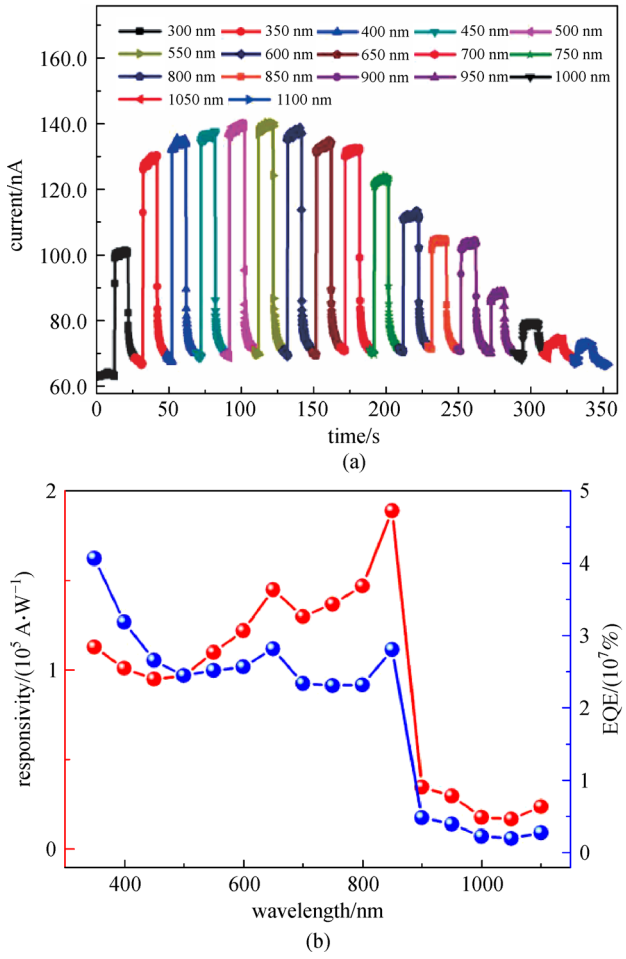

Fig. 4 (a) Photoresponse characteristics and (b) responsivity (left) and EQE (right) of the device to light illuminations with different wavelengths ranging from UV to NIR regions at a bias of 1 V

with narrow direct band gap of 1.3 eV (corresponding to 930 nm) [23–25], theoretically In_2Se_3 has photosensitivity to UV-visible-NIR lights. We further studied the photoresponse of the longitudinal twinning In_2Se_3 nanowires under incident light illumination in the UV-visible-NIR range, as shown in Fig. 4(a). Here, the wavelength of the homochromatic light is continuously tuned by a monochromator varied from 300 to 1100 nm with an interval of 50 nm. As expected, the demonstrated photoresponse appears to be high across the broad spectra from 300 nm to 1100 nm. In addition, the *I-V* curves under light illuminations with different wavelengths are plotted in Fig. S4. All the curves exhibit linear behaviors, suggesting a good ohmic contact between Ti/Au electrodes and the In_2Se_3 nanowires. Figure 4(b) shows the responsivity (left) and EQE (right) under light illumination with different wavelengths at a basis of 1 V. In the 350 – 850 nm regions, the measured responsivity is as high as 10^5 A·W^{-1}, and the calculated EQE is as high as 10^7%. As the incident light wavelength further increased, responsivity and EQE slowly decrease by an order of magnitude, with responsivity at 10^4 A·W^{-1} and EQE at 10^6% in the 850 – 1100 nm regions. Besides, when the wavelength of incident light is 300 nm, the responsivity and EQE is as high as 9.82×10^5 A·W^{-1} and 41.3×10^8%, which may originate from the absorption and desorption process of gas molecules on the surface of the In_2Se_3 nanowire under UV light [14]. The above results proved that the longitudinal twinning In_2Se_3 nanowires have a high response to UV, visible, NIR.

We also measured the current-time (*I-T*) curves for two ON/OFF cycles under 300 and 800 nm lights irradiation with different power intensities at a bias voltage of 1 V, as shown in Figs. S5(a) and S5(c), respectively. It can be seen that, for both wavelengths, the saturation photocurrent decreases as the light intensity decreases, and then returns to the same value as the light intensity recovery, indicating that the photodetector has good reproducibility. Figures S5 (b) and S5(d) show the photocurrent and responsivity as a function of light power intensity for 300 nm light irradiation at V_{ds} = 1 V and 800 nm light irradiation at V_{ds} = 3 V, respectively. The fitting results are I_{ph}~$P^{0.97}$ and I_{ph}~$P^{0.94}$, where *r* values are 0.97 and 0.94, respectively. Combined with the data in Fig. 3(d), the results show that the In_2Se_3 nanowire photodetectors have good photocurrent effect under UV, visible and NIR illuminations. And R_λ deceases as the power intensity of light increases, which is the same as the trend in visible light range.

The time-resolved photoresponse performance of the twinning In_2Se_3 based photodetectors under various wavelength are measured, as shown in Figs. 5(a) – 5(f), corresponding to the lights with the wavelengths of 300, 400, 500, 700, 800 and 900 nm, respectively. From these results, we can see that the photodetectors demonstrate reversible and stable photoresponse properties under the measured wavelengths by periodically switching the lights on and off, which verify the outstanding stability of our devices for wide wavelengths from UV, visible to NIR lights. Furthermore, Fig. 5(g) presents a single cycle wavelength-dependent time-resolved responses of the device to lights with the wavelengths ranging from 300 to 900 nm. The device show fast response and recovery time to all the measured lights. The corresponding measured response time and recovery time are all about 0.11 and 0.6 s, indicating that the longitudinal twinning In_2Se_3-based photodetector shows excellent sensitivity to lights ranging from UV, visible, to NIR.

We also compared the key device performance figures-of-merit of our device with previously reported In_2Se_3-nanostructures based devices, as listed in Table 1. From these data, we can see that our current longitudinal twinning α-In_2Se_3 nanowire based device exhibits higher photocurrent, higher spectral responsivity and higher detectivity compared with other reported In_2Se_3-nanostructures devices. Such improved properties are thought to

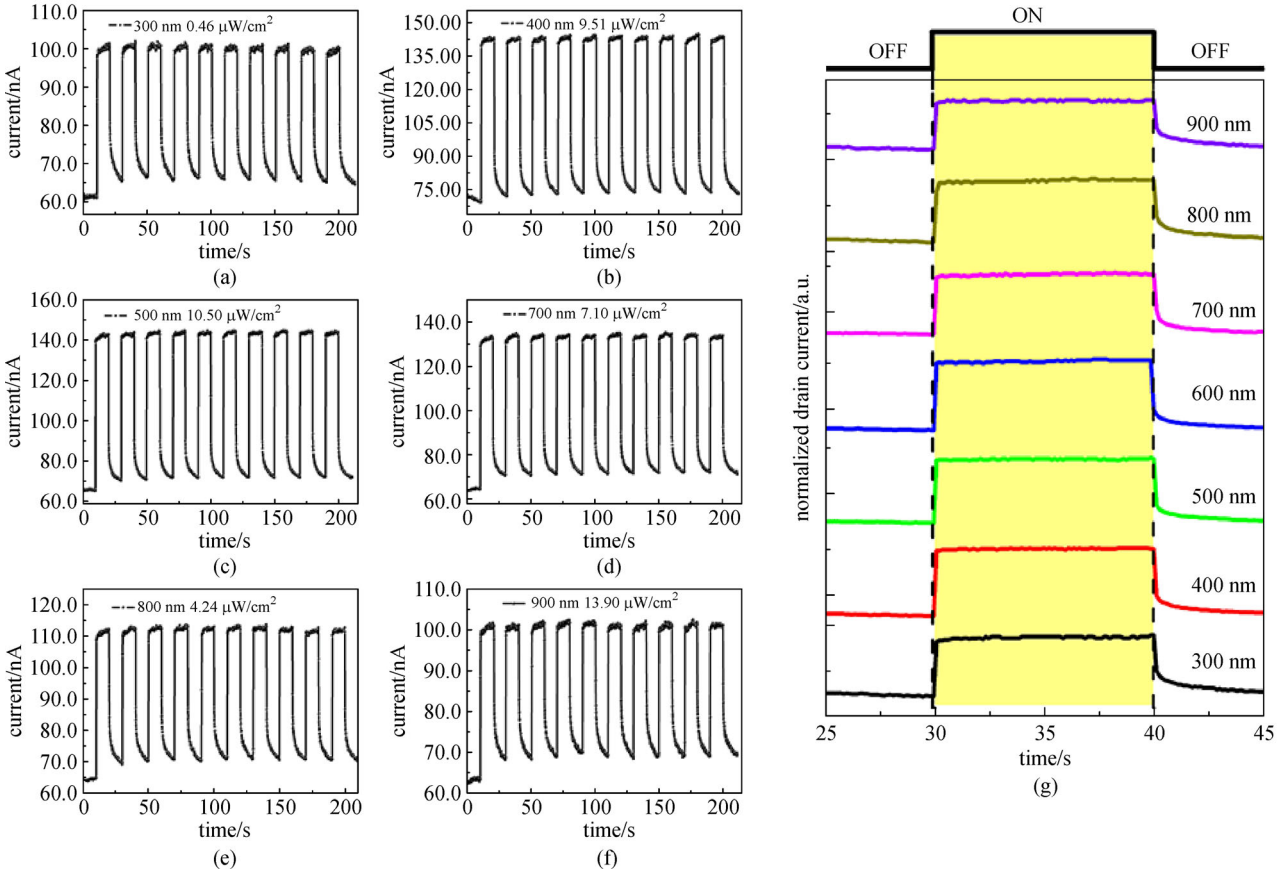

Fig. 5 Time-resolved photoresponse performance of the In_2Se_3 nanowires device illuminated under (a) 300 nm, (b) 400 nm, (c) 500 nm, (d) 700 nm, (e) 800 nm, and (f) 900 nm by switching the light on and off at a bias of 1 V, respectively. (g) Photoresponse times under various excitation wavelengths

Table 1 Comparison of the key device performance figures-of-merit for the reported In_2Se_3-nanostructures based photodetectors

photodetectors	measurement condition	I_{ph}/A	spectral range/nm	responsivity/(A·W^{-1})	detectivity(D^*)/Jones	source
α-In_2Se_3 NWs	500 nm, 3 V	200 p	–	89	–	[15]
γ-In_2Se_3 microwires	633 nm, 4 V	8 n	365 – 1050	0.54	3.94×10^{10}	[20]
S-doped In_2Se_3 NWs	500 nm, 3 V	130 n	–	1331	–	[45]
In_2Se_3 nanosheets	500 nm, 5 V	20 p	300 – 1100	59	3.37×10^{11}	[46]
α-In_2Se_3 twinning NWs	600 nm,3 V	165 n	300 – 1100	4.18×10^5	1.58×10^{12}	this work

be the result of the special structure of the twinning nanowires. It is known that the conduction of In_2Se_3 nanowires mainly originates from Se vacancies that are native donors [15]. For conventional single crystalline In_2Se_3 nanowire, it usually has lower conductivity due to a higher crystal quality and few defects sites. However, for the twinning nanowires in this work, the twin, as one of the most important kinds of defects, can bring more Se vacancies. Hence, the twinning In_2Se_3 nanowire has a higher conductivity. Besides, the twin plane of the longitudinal twinning nanowire is parallel to the current conduction direction, which on one hand, does not impede the conduction of the current. It also acts as a current channel on another hand. Because of all these factors, the longitudinal twinning α-In_2Se_3 nanowires exhibit improved photoresponse performance compared with other kinds of In_2Se_3 nanostructures.

4 Conclusions

In summary, by controlling the growth temperature and Ar gas flow, longitudinal twinning α-In_2Se_3 nanowires with diameters of 100 – 300 nm and lengths of several tens of micrometers are fabricated by a CVD method. The twining nanowires have the (1018) twin planes parallel to the axis of the nanowires. To explore the effect of the special twinning structure on the optoelectronic characteristics,

single nanowire photodetectors are fabricated, which exhibited typical n-type semiconducting behavior with an electron mobility of 23.1 $cm^2 \cdot V^{-1} \cdot S^{-1}$ and a broadband spectral response with high responsivity, stability, and reproducibility with the light wavelengths ranging from 300 to 1100 nm, covering the UV-visible-NIR region. The R_λ, EQE and D^* could reach up to 8.57×10^5 $A \cdot W^{-1}$, 8.8×10^7% and 1.58×10^{12} Jones under 600 nm light illumination at a basis of 3 V, superior to other reported In_2Se_3 nanostructures based photodetectors. These results prove that the longitudinal twinning In_2Se_3 nanowires may have immense potential for future applications in the highly sensitive and stable broadband spectral detectors and other related optoelectronic devices.

Acknowledgements This work was financially supported by the National Natural Science Foundation of China (NSFC) (Grant Nos. 61625404, 61574132), and the Key Research Program of Frontier Sciences, CAS (No. QYZDY-SSW-JWC004).

Author contributions Z. D. Zhang and J. H. Yang performed the experiments; all authors contributed to the general discussion and have given approval to the final version of the paper.

Conflict of interest The authors declare that they have no conflict of interest.

Supporting Information

TEM, XPS data of In_2Se_3-based twinning nanowires and the photoresponse data of the In_2Se_3-based photodetectors are shown in Figs. S1 – S5.

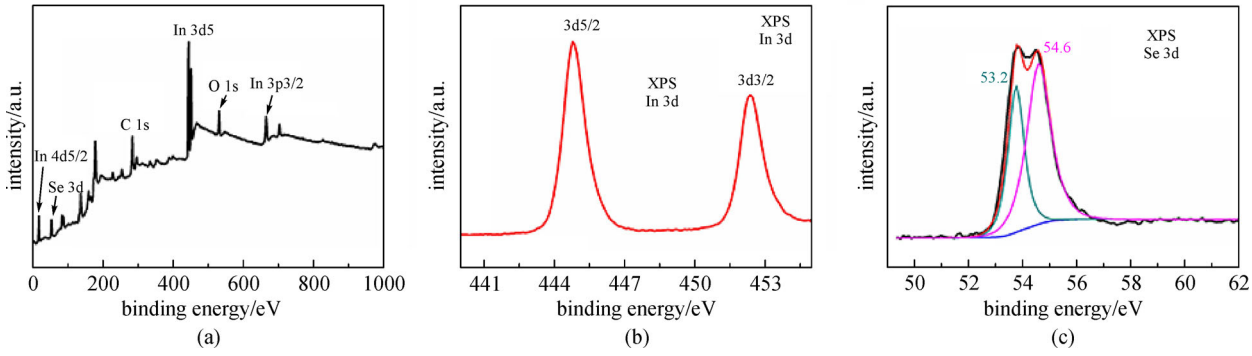

Figs. S1 (a) Full scale XPS scan, (b) in peaks, and (c) Se 3d doublets of the synthesized α-In_2Se_3 nanowires

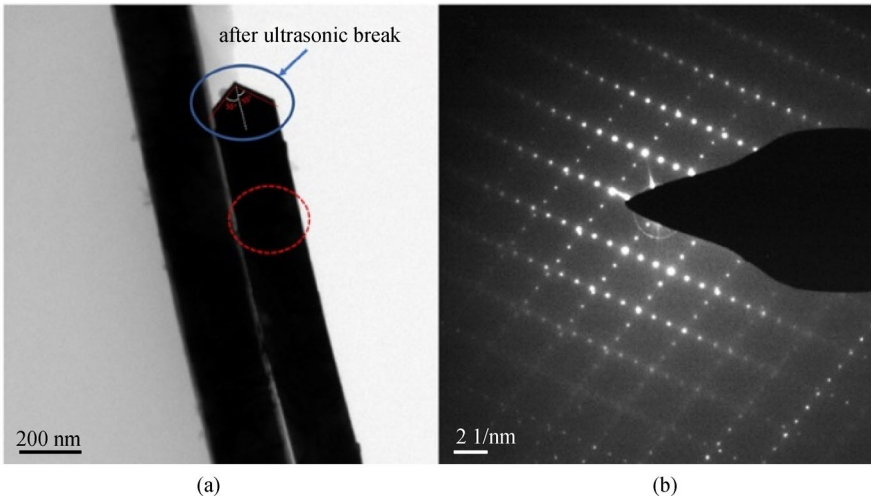

Figs. S2 (a) TEM image, and (b) SAED pattern of the synthesized twinned α-In_2Se_3 nanowires

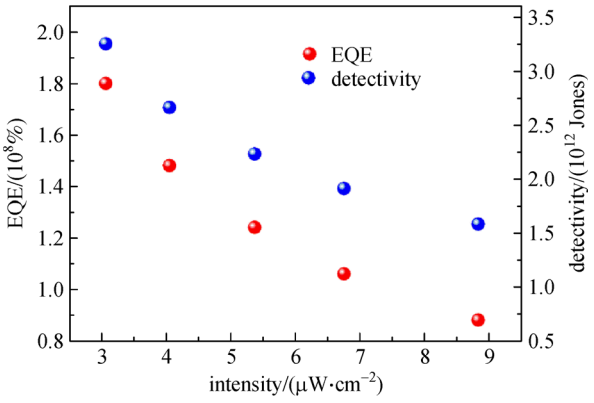

Figs. S3 Key device figures-of-merit, EQE and specific detectivity of the devices measured at different power intensities of 600 nm light illumination at a 3 V bias

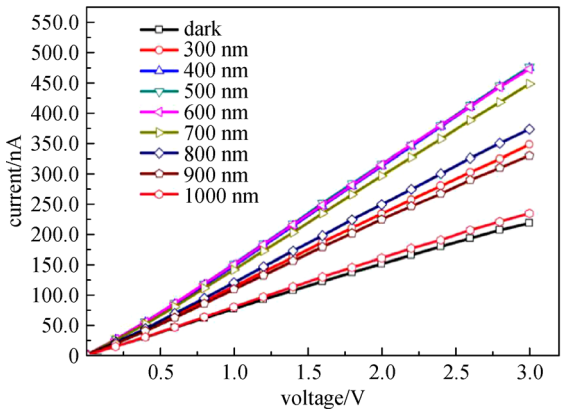

Figs. S4 *I-V* curves of the device illuminated with incident light of various wavelengths and in the dark, respectively

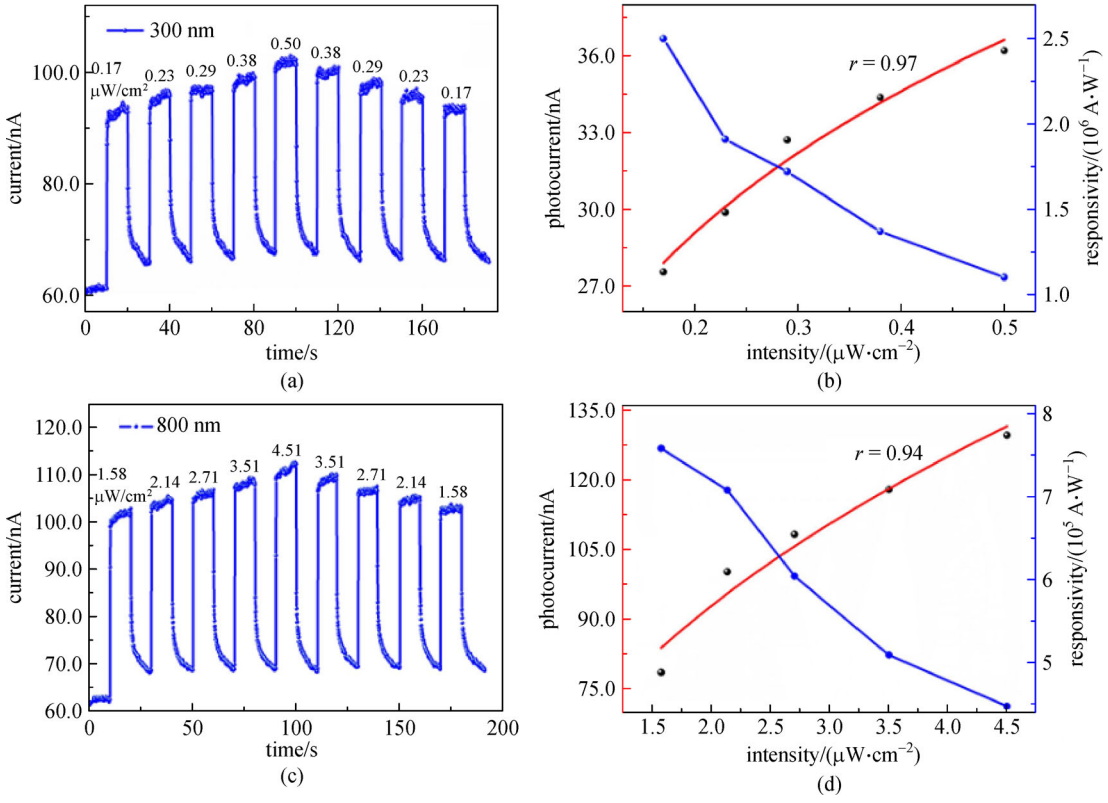

Figs. S5 (a) Time-resolved photoresponse characteristics of the device at a bias of 1 V in 300 nm with different light intensities. (b) Photocurrent and responsivity as a function of light power intensity in 300 nm. The fitting result is I_{ph}~$P^{0.97}$. (c) Time-resolved photoresponse characteristics of the device at a bias of 3 V in 800 nm with different light intensities. (d) Photocurrent and responsivity as a function of light power intensity in 300 nm. The fitting result is I_{ph}~$P^{0.94}$

References

1. Fan Z, Ho J C, Jacobson Z A, Razavi H, Javey A. Large-scale, heterogeneous integration of nanowire arrays for image sensor circuitry. Proceedings of the National Academy of Sciences of the United States of America, 2008, 105(32): 11066–11070
2. Li L, Gu L, Lou Z, Fan Z, Shen G. ZnO quantum dot decorated Zn_2SnO_4 nanowire heterojunction photodetectors with drastic performance enhancement and flexible ultraviolet image sensors. ACS Nano, 2017, 11(4): 4067–4076
3. Kind H, Yan H, Messer B, Law M, Yang P. NW ultraviolet photodetectors and optical switches. Advanced Materials, 2002, 14 (2): 158–160
4. Ju S, Facchetti A, Xuan Y, Liu J, Ishikawa F, Ye P, Zhou C, Marks T

J, Janes D B. Fabrication of fully transparent nanowire transistors for transparent and flexible electronics. Nature Nanotechnology, 2007, 2(6): 378–384
5. Yoo J, Jeong S, Kim S, Je J H. A stretchable nanowire UV-Vis-NIR photodetector with high performance. Advanced Materials, 2015, 27(10): 1712–1717
6. Wang Z, Wang H, Liu B, Qiu W, Zhang J, Ran S, Huang H, Xu J, Han H, Chen D, Shen G. Transferable and flexible nanorod-assembled TiO_2 cloths for dye-sensitized solar cells, photodetectors, and photocatalysts. ACS Nano, 2011, 5(10): 8412–8419
7. Lou Z, Li L, Shen G. High-performance rigid and flexible ultraviolet photodetectors with single-crystalline $ZnGa_2O_4$ nanowires. Nano Research, 2015, 8(7): 2162–2169
8. Park C M, Sohn H J. Quasi-intercalation and facile amorphization in layered ZnSb for Li-ion batteries. Advanced Materials, 2010, 22(1): 47–52
9. Liu B, Zhang J, Wang X, Chen G, Chen D, Zhou C, Shen G. Hierarchical three-dimensional $ZnCo_2O_4$ nanowire arrays/carbon cloth anodes for a novel class of high-performance flexible lithium-ion batteries. Nano Letters, 2012, 12(6): 3005–3011
10. Wang Y, Jiang X, Xia Y. A solution-phase, precursor route to polycrystalline SnO2 nanowires that can be used for gas sensing under ambient conditions. Journal of the American Chemical Society, 2003, 125(52): 16176–16177
11. Liu X, Liu X, Wang J, Liao C, Xiao X, Guo S, Jiang C, Fan Z, Wang T, Chen X, Lu W, Hu W, Liao L. Transparent, high-performance thin-film transistors with an InGaZnO/aligned-SnO_2 -nanowire composite and their application in photodetectors. Advanced Materials, 2014, 26(43): 7399–7404
12. Feng G, Yang C, Zhou S. Nanocrystalline Cr^{2+}-doped ZnSe nanowires laser. Nano Letters, 2013, 13(1): 272–275
13. Xie X, Shen G. Single-crystalline In_2S_3 nanowire-based flexible visible-light photodetectors with an ultra-high photoresponse. Nanoscale, 2015, 7(11): 5046–5052
14. Wang Z, Safdar M, Jiang C, He J. High-performance UV-visible-NIR broad spectral photodetectors based on one-dimensional In_2Te_3 nanostructures. Nano Letters, 2012, 12(9): 4715–4721
15. Zhai T, Fang X, Liao M, Xu X, Li L, Liu B, Koide Y, Ma Y, Yao J, Bando Y, Golberg D. Fabrication of high-quality In_2Se_3 nanowire arrays toward high-performance visible-light photodetectors. ACS Nano, 2010, 4(3): 1596–1602
16. Peng H, Zhang X F, Twesten R D, Cui Y. Vacancy ordering and lithium insertion in III_2VI_3 nanowires. Nano Research, 2009, 2(4): 327–335
17. Xu J, Luan C Y, Tang Y B, Chen X, Zapien J A, Zhang W J, Kwong H L, Meng X M, Lee S T, Lee C S. Low-temperature synthesis of $CuInSe_2$ nanotube array on conducting glass substrates for solar cell application. ACS Nano, 2010, 4(10): 6064–6070
18. Julien C, Hatzikraniotis E, Chevy A, Kambas K. Electrical behavior of lithium intercalated layered In-Se compounds. Materials Research Bulletin, 1985, 20(3): 287–292
19. Li Q, Li Y, Gao J, Wang S, Sun X. High performance single In_2Se_3 nanowire photodetector. Applied Physics Letters, 2011, 99(24): 243105–243109
20. Ali Z, Mirza M, Cao C, Butt F K, Tanveer M, Tahir M, Aslam I, Idrees F, Safdar M. Wide range photodetector based on catalyst free grown indium selenide microwires. ACS Applied Materials & Interfaces, 2014, 6(12): 9550–9556
21. Kang D, Rim T, Baek C K, Meyyappan M, Lee J S. Thermally phase-transformed In_2Se_3 nanowires for highly sensitive photodetectors. Small, 2014, 10(18): 3795–3802
22. Peng H, Schoen D T, Meister S, Zhang X F, Cui Y. Synthesis and phase transformation of In_2Se_3 and $CuInSe_2$ nanowires. Journal of the American Chemical Society, 2007, 129(1): 34–35
23. Jasinski J, Swider W, Washburn J, Liliental-Weber Z, Chaiken A, Nauka K, Gibson G A, Yang C C. Crystal structure of κ-In_2Se_3. Applied Physics Letters, 2002, 81(23): 4356–4358
24. Lakshmikumar S T, Rastogi A C. Selenization of Cu and In thin films for the preparation of selenide photo-absorber layers in solar cells using Se vapour source. Solar Energy Materials and Solar Cells, 1994, 32(1): 7–19
25. Lai K, Peng H, Kundhikanjana W, Schoen D T, Xie C, Meister S, Cui Y, Kelly M A, Shen Z X. Nanoscale electronic inhomogeneity in In_2Se_3 nanoribbons revealed by microwave impedance microscopy. Nano Letters, 2009, 9(3): 1265–1269
26. Yu B, Ju S, Sun X H, Ng G, Nguyen T D, Meyyappan M, Janes D B. Indium selenide nanowire phase-change memory. Applied Physics Letters, 2007, 91(13): 133119–133121
27. Algra R E, Verheijen M A, Borgström M T, Feiner L F, Immink G, van Enckevort W J, Vlieg E, Bakkers E P. Twinning superlattices in indium phosphide nanowires. Nature, 2008, 456(7220): 369–372
28. Grap T, Rieger T, Blömers Ch, Schäpers T, Grützmacher D, Lepsa M I. Self-catalyzed VLS grown InAs nanowires with twinning superlattices. Nanotechnology, 2013, 24(33): 335601
29. Algra R E, Verheijen M A, Feiner L F, Immink G G W, Enckevort W J, Vlieg E, Bakkers E P A M. The role of surface energies and chemical potential during nanowire growth. Nano Letters, 2011, 11 (3): 1259–1264
30. Burgess T, Breuer S, Caroff P, Wong-Leung J, Gao Q, Hoe Tan H, Jagadish C. Twinning superlattice formation in GaAs nanowires. ACS Nano, 2013, 7(9): 8105–8114
31. Meng Q, Jiang C, Mao S X. Temperature-dependent growth of zinc-blende-structured ZnTe nanostructures. Journal of Crystal Growth, 2008, 310(20): 4481–4486
32. Hao Y, Meng G, Wang Z L, Ye C, Zhang L. Periodically twinned nanowires and polytypic nanobelts of ZnS: the role of mass diffusion in vapor-liquid-solid growth. Nano Letters, 2006, 6(8): 1650–1655
33. Wang J, Sun X W, Xie S, Zhou W, Yang Y. Single-crystal and twinned Zn_2SnO_4 nanowires with axial periodical structures. Crystal Growth & Design, 2008, 8(2): 707–710
34. Kim H S, Myung Y, Cho Y J, Jang D M, Jung C S, Park J, Ahn J P. Three-dimensional structure of twinned and zigzagged one-dimensional nanostructures using electron tomography. Nano Letters, 2010, 10(5): 1682–1691
35. Xu J, Lu A J, Wang C, Zou R, Liu X, Wu X, Wang Y, Li S, Sun L, Chen X, Oh H, Baek H, Yi G, Chu L. ZnSe-based longitudinal twinning nanowires. Advanced Engineering Materials, 2014, 16(4): 459–465
36. Xu J, Wang C, Zhang Y, Liu X, Liu X, Huang S, Chen X. Structural, vibrational and luminescence properties of longitudinal twinning Zn_2GeO_4 nanowires. CrystEngComm, 2013, 15(4): 764–768

37. Ikonić Z, Srivastava G P, Inkson J C. Electronic properties of twin boundaries and twinning superlattices in diamond-type and zinc-blende-type semiconductors. Physical Review B: Condensed Matter, 1993, 48(23): 17181–17193
38. Tsuzuki H, Cesar D F, Dias M R, Castelano L K, Lopez-Richard V, Rino J P, Marques G E. Tailoring electronic transparency of twin-plane 1D superlattices. ACS Nano, 2011, 5(7): 5519–5525
39. Akiyama T, Yamashita T, Nakamura K, Ito T. Band alignment tuning in twin-plane superlattices of semiconductor nanowires. Nano Letters, 2010, 10(11): 4614–4618
40. Shimamura K, Yuan Z, Shimojo F, Nakano A. Effects of twins on the electronic properties of GaAs. Applied Physics Letters, 2013, 103(2): 022105–022109
41. Johansson J, Karlsson L S, Svensson C P T, Mårtensson T, Wacaser B A, Deppert K, Samuelson L, Seifert W. Structural properties of < 111 > B-oriented III-V nanowires. Nature Materials, 2006, 5 (7): 574–580
42. Shen G, Xu J, Wang X, Huang H, Chen D. Growth of directly transferable In_2O_3 nanowire mats for transparent thin-film transistor applications. Advanced Materials, 2011, 23(6): 771–775
43. Shao D, Gao J, Chow P, Sun H, Xin G, Sharma P, Lian J, Koratkar N A, Sawyer S. Organic–inorganic heterointerfaces for ultrasensitive detection of ultraviolet light. Nano Letters, 2015, 15(6): 3787–3792
44. Fonoberov V A, Balandin A A. ZnO quantum dots: physical properties and optoelectronic applications. Journal of Nanoelectronics and Optoelectronics, 2006, 1(1): 19–38
45. Zhai T, Ma Y, Li L, Fang X, Liao M, Koide Y, Yao J, Bando Y, Golberg D. Morphology-tunable In_2Se_3 nanostructures with enhanced electrical and photoelectrical performances via sulfur doping. Journal of Materials Chemistry, 2010, 20(32): 6630–6637
46. Jacobs-Gedrim R B, Shanmugam M, Jain N, Durcan C A, Murphy M T, Murray T M, Matyi R J, Moore R L 2nd, Yu B. Extraordinary photoresponse in two-dimensional In_2Se_3 nanosheets. ACS Nano, 2014, 8(1): 514–521

Zidong Zhang received his B.Sc. degree from School of Material Science and Engineering, Nanchang Hangkong University, China, in 2015. Now he is a master student in the Research Center of Advanced Materials Science and Technology, Taiyuan University of Technology, China. His research interest focuses on investigation of optoelectronic properties of low-dimensional semiconductor materials.

Juehan Yang received his Ph.D. degree in 2016 for condensed matter physics at Institute of Semiconductors, Chinese Academy of Sciences. Since 2016, he has worked at Institute of Semiconductors as an assistant professor. His research field in optical and electrical properties of low dimensional materials.

Fuhong Mei received his B.Sc. degree in applied physics from the Department of Applied Physics, Northwestern Polytechnical University and Ph.D. degree in condensed matter physics from the School of Physics, Peking University, China, in 2006 and 2013, respectively. He has since 2013 been a faculty member of the Research Center of Advanced Materials Science and Technology, Taiyuan University of Technology, China. His main research interests include the investigation of optoelectronic properties of low-dimensional semiconductor materials via surface modification treatment, innovated structures and the like to reveal the hidden mechanism therein.

Guozhen Shen received his B.Sc. degree in 1999 from Anhui Normal University and Ph.D. degree in 2003 from the University of Science and Technology of China. From 2004 to 2009, he conducted his research in Hanyang University (Korea), National Institute for Materials Science (Japan), University of Southern California (USA) and Huazhong University of Science and technology. He joined the Institute of Semiconductors, Chinese Academy of Sciences as a professor in 2013. His current research focuses on flexible electronics and printable electronics, including transistors, photodetectors, sensors and flexible energy-storage devices.